Improving the binding efficiency of quartz crystal microbalance biosensors by applying the electrothermal effect

Yao-Hung Huang, Jeng-Shian Chang, Sheng D. Chao, Kuang-Chong Wu, and Long-Sun Huang

Citation: Biomicrofluidics **8**, 054116 (2014); doi: 10.1063/1.4898633
View online: http://dx.doi.org/10.1063/1.4898633
View Table of Contents: http://scitation.aip.org/content/aip/journal/bmf/8/5?ver=pdfcov
Published by the AIP Publishing

Improving the binding efficiency of quartz crystal microbalance biosensors by applying the electrothermal effect

Yao-Hung Huang, Jeng-Shian Chang,[a] Sheng D. Chao, Kuang-Chong Wu, and Long-Sun Huang
Institute of Applied Mechanics, National Taiwan University, Taipei, Taiwan

(Received 2 September 2014; accepted 6 October 2014; published online 15 October 2014)

A quartz crystal microbalance (QCM) serving as a biosensor to detect the target biomolecules (analytes) often suffers from the time consuming process, especially in the case of diffusion-limited reaction. In this experimental work, we modify the reaction chamber of a conventional QCM by integrating into the multi-microelectrodes to produce electrothermal vortex flow which can efficiently drive the analytes moving toward the sensor surface, where the analytes were captured by the immobilized ligands. The microelectrodes are placed on the top surface of the chamber opposite to the sensor, which is located on the bottom of the chamber. Besides, the height of reaction chamber is reduced to assure that the suspended analytes in the fluid can be effectively drived to the sensor surface by induced electrothermal vortex flow, and also the sample costs are saved. A series of frequency shift measurements associated with the adding mass due to the specific binding of the analytes in the fluid flow and the immobilized ligands on the QCM sensor surface are performed with or without applying electrothermal effect (ETE). The experimental results show that electrothermal vortex flow does effectively accelerate the specific binding and make the frequency shift measurement more sensible. In addition, the images of the binding surfaces of the sensors with or without applying electrothermal effect are taken through the scanning electron microscopy. By comparing the images, it also clearly indicates that ETE does raise the specific binding of the analytes and ligands and efficiently improves the performance of the QCM sensor. © *2014 AIP Publishing LLC*. [http://dx.doi.org/10.1063/1.4898633]

I. INTRODUCTION

In recent years, biosensors for monitoring patients outside the hospital have been vigorously developed. Their advantages include low cost, rapid detection, and miniaturization.[1–3] Therefore, experts of relevant fields have focused on developing biosensors as for next-generation detection technology. Compared to conventional biomedical testing equipment, miniaturized detection systems are more portable. However, the required time of a specific biomolecular recognition usually depends on its Damköhler number (Da number), which is a dimensionless parameter to measure whether a reaction is diffusion-limited or reaction rate-limited. The Da number is the ratio of reaction velocity (i.e., product of the association rate constant and the initial concentration of the ligand) to diffusion velocity (i.e., ratio of the diffusion coefficient of the analyte in the buffer flow to the height of microchannel).[4] When the Da number is greater than unity, the whole reaction is restrained by diffusion. Although the reaction kinetics of antigen–antibody binding in microfluidic chips where the diffusion distance is not great, the Da number can be on the order of 100 or higher.[5,6] The binding of analytes and

[a]Author to whom correspondence should be addressed. Electronic mail: jschang@iam.ntu.edu.tw. Tel.: +886-2-33665678. Fax: +886-2-23639290.

immobilized ligands in the sensor of the microsystem causes slow binding of analyte molecules in the flow and immobilizes ligand molecules on the reaction surface, due to the diffusion boundary layer on the reaction surface in the case of diffusion-limited reaction.[7,8] Due to the micro size of the sensor, it is hard to stir the flow in the reaction cell by applying conventional external force. In contrast, the AC electrokinetic method[9,10] is particularly effective in the micro-nano domain and can be easily integrated with other microfluidic components. Additionally, different fluidic operations can be realized in a single platform by inducing electrokinetics such as concentration, focusing, separation, mixing, and pumping.[11–15] With many applications already in use in the biomechanics field, the electrokinetic method has the greatest potential for use in microfluidic diagnosis systems.[16]

The three main AC electrokinetic phenomena are dielectrophoresis (DEP), AC electroosmosis (ACEO), and electrothermal effect (ETE).[17] Dielectrophoresis often involves microparticles such as cells[18] or bacteria.[19] However, dielectrophoresis may be ineffective for examining experimental specimens, which are often nanosize antibodies (proteins) or drug molecules. ACEO and ETE can generate micro vortices to achieve mixing effect. Generally, ACEO operates at low frequency (below 100 kHz) in a low-conductivity solution,[20] whereas ETE works at a high frequency (above 100 kHz) in a high-conductivity solution (above 0.002 S/m) (Refs. 21 and 22). Since specimens are usually electrolyte-rich solutions with high conductivity, ACEO specimens must be converted into solutions with low conductivity, which limits their activity and viability. By contrast, specimens employed in electrothermal processes are compatible with their surrounding electrical field. Since no pretreatment is required, ETE is suitable for biosensing processes. ETE uses microelectrodes to create non-uniform electric fields, which produce local Joule heating around the electrodes. Thus, uneven temperature T distribution in the flow field space changes the dielectric coefficient ε and conductivity σ gradient of the fluid, thereby forming Coulomb force and dielectric force. The equation for electrothermal force is as follows:[23]

$$\vec{F}_{ETE} = -0.5\left[\left(\frac{\nabla\sigma}{\sigma} - \frac{\nabla\varepsilon}{\varepsilon}\right)\cdot\vec{E}\,\frac{\varepsilon\vec{E}}{1+(\omega\tau)^2} + 0.5|\vec{E}|^2\nabla\varepsilon\right], \tag{1}$$

where $\tau = \varepsilon/\sigma$ is the charge relaxation time of the fluid and ω represents the angular frequency required for electric field E. In this equation, the first and second terms on the right are the Coulomb force and dielectric force, respectively. The Coulomb force is dominant at low frequency, whereas the dielectric force is dominant at high frequency. Moreover, the crossover frequency of the buffer solution used in this study (conductivity $\sigma = 1.45\ S/m$) was approximately 1.1 GHz.[17] The conductivity and frequency (10 MHz) used in this study are both considerably high, hence the ACEO is neglected.[24,25]

Parts of previous studies[26–32] adopted numerical models to verify the feasibility of using electrokinetic in developing flow field-based mixing sensors. In contrast, numbers of studies performed experimental explorations.[33–35] Feldman *et al.*[33] placed microelectrodes on both sides of the binding region to introduce electrothermal stirring to increase the binding probability of fluorescently labeled streptavidin and biotin. Hart *et al.*[34] modified a circular electrode in a quartz crystal microbalance (QCM) for a pair of interdigitated electrodes. The electrothermal force produced by the modification, improved the capture of immunoglobulin G (IgG) and the overall performance of the biosensor. Ouyang *et al.*[35] applied ETE to generate a mixing effect that enhanced the bacteria detection sensitivity and overall performance of an electrochemical biosensor by enhancing biomolecular convection and hybridization efficiency. Most of the above reported experiments were performed using dip and dry method, in which the detected analytes were pipetted onto the sensing area, cleaned and blow dried after the binding step, and then returned to the gas phase for measurement of the biosensor signal.[34–36]

In this work a local made QCM was adopted as biosensor because of its simple structure, durability, and stability. QCM has numerous nanoscale sensor applications, including detection of DNA hybridizations,[37] antibody interactions,[38,39] viruses,[40] cells,[41] drugs,[42] and heavy metal

ions.[43] Electrothermal microelectrodes were integrated in the QCM chip. Electrothermally induced vortices caused rapid migration of analytes in the fluid of the chamber toward the reaction surface of the QCM, and hence disintegrated the diffusion boundary layer due to limited diffusion. The biosensor was then employed to directly measure the electrothermal signals in liquid phase without performing fluorescent labeling. Finally, particles of two sizes and various concentrations in the presence and absence of electrothermal stirring were examined and compared through the frequency shifts and the immobilized sensor surface density from the images taken by scanning electron microscopy (SEM).

II. EXPERIMENTS

A. ETE-QCM setup

Figure 1(a) shows the schematic concept of the QCM reaction chamber with only two pairs of electrodes shown for clear illustration (eight pairs in actual setup). The microelectrodes and the sensing electrodes of the QCM chip were placed on the top and bottom walls of the sensing chamber, respectively.

The ETE-QCM chip consisted of the microelectrodes (top part), the optical clear adhesive (middle part), and the QCM sensor (bottom part). Figure 1(b) shows the schematic illustration

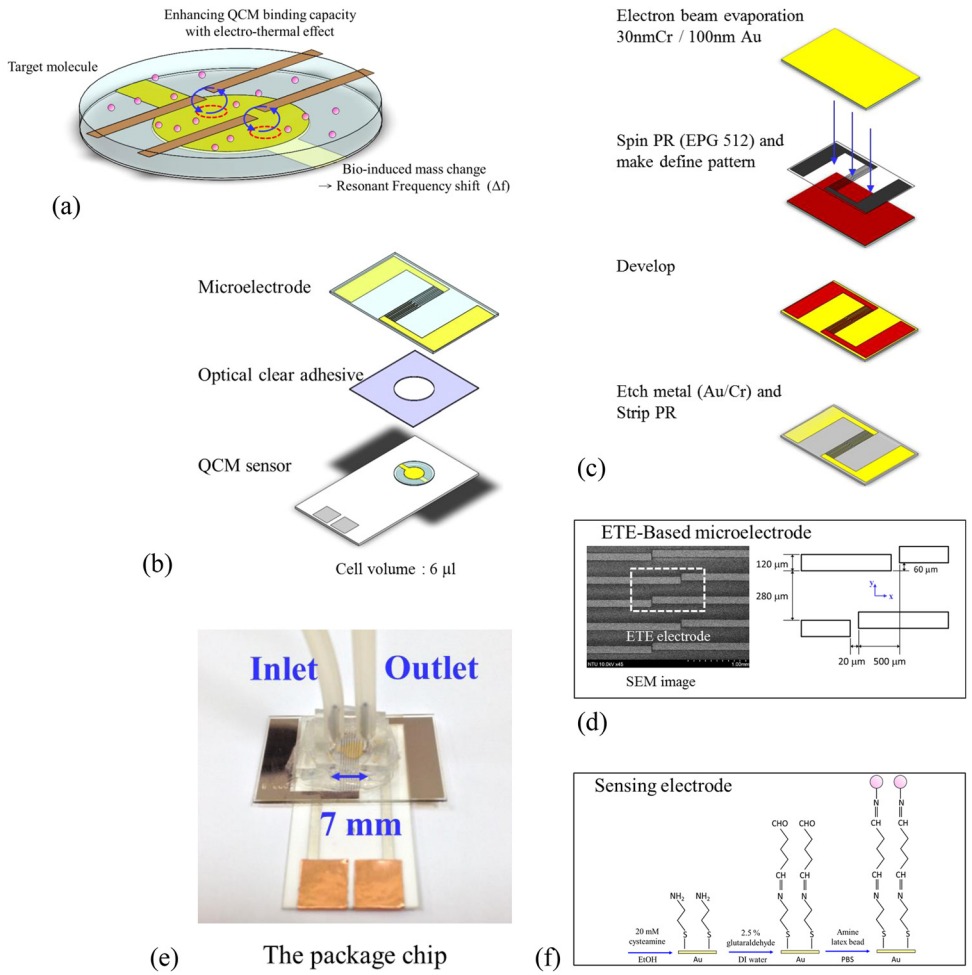

FIG. 1. (a) Illustration of ETE-QCM technique. The top electrothermal electrode forms vortices that transfer analytes downward to the bottom sensing electrode. (b) Illustration of ETE-QCM chips. (c) Micro-fabrication processes of the ETE chip with multi-microelectrodes. (d) Geometry and SEM image of the microelectrode. (e) Assembly of ETE-QCM chips. (f) Schematic diagram of amine latex beads immobilization strategy used in the QCM sensing electrode.

of ETE-QCM chip. First, the top microelectrodes for generating electrothermal flow were attached to a glass substrate cleaned with piranha solution (H_2SO_4:H_2O_2 = 3:1). A 30 nm chrome (Cr) adhesion layer and a 100 nm gold (Au) layer were deposited on the glass substrate with an E-beam evaporator. Photolithography was applied with a photoresist EPG 512 (Everlight Chemical Industrial Corp., Taiwan) to generate an electrode pattern, and then remove the unmasking layer of Au and Cr sequentially by Au etchants and Cr etchants. Figure 1(c) shows the schematic illustration of the micro-fabrication processes. Overall, eight pairs of electrodes were fabricated. The gap between the components of each pair was 20 μm. Figure 1(d) then shows the detailed geometric dimensions and the arrangements of the electrodes. Each pair of electrodes was arranged 60 μm offset in a longitudinal direction (y-axis) for the purpose of creating a stronger non-uniform electric field. Neighboring electrode pairs were installed at 500 μm (x-axis) apart on the bottom left or on the bottom right. After cutting each chip into 29 mm × 18 mm × 0.5 mm pieces with a precision dicing saw (DS-150 II, Disco, Japan), two 1-mm diameter holes were drilled in the chip to provide an inlet and outlet for fluids. The middle part was a circular reaction chamber, with a 7 mm diameter hole, formed by optically clear adhesive (OCA) tape. The bottom QCM sensor and the top microelectrode were then aligned and well bonded with OCA tape. Figure 1(e) shows the completed ETE-QCM chip. Measurements with a white light interferometer (BMT, Germany) showed that the thickness of the OCA tape was 150 μm, and that the inner volume of the reaction chamber was 6 μl.

Figure 2 shows the components of the biosensing platform, which comprised a microfluidic system, an ETE-QCM chip, a function generator, and a detection system. The ETE-QCM chip was connected to a programmable syringe pump (NE-300; New Era Pump systems, Inc., USA) and an injection valve (7725i; Rheodyne, USA), through which samples were injected. The AC voltage used to produce electrothermal force was supplied by a synthesized function generator (DS 345; Stanford Research Systems, CA, USA). In the Affinity Detection System (ANT Technologies Corp., Taiwan), the resonance frequency was recorded using a frequency counter and directly displayed on the computer screen. The resolution was 0.1 Hz, and recordings were made every second.

B. Reagents and materials

The 30 % hydrogen peroxide (H_2O_2), 98 % sulfuric acid (H_2SO_4), and hydrogen chloride (HCL) used in the experiments were purchased from Asia Union Electronical Chemical Corp (Taiwan). The sodium hydroxide (NaOH), Cr etchant, Gold etchant, and the reagents, cysteamine (HS-$(CH_2)_2$-NH_2), glutaraldehyde (OHC-$(CH_2)_3$-CHO), phosphate-buffered saline (PBS, pH 7.4,), and pure ethanol (>99.8 %) were purchased form Sigma Aldrich (USA). Amine latex beads were purchased from Invitrogen Molecular Probes (USA). The density of amine latex

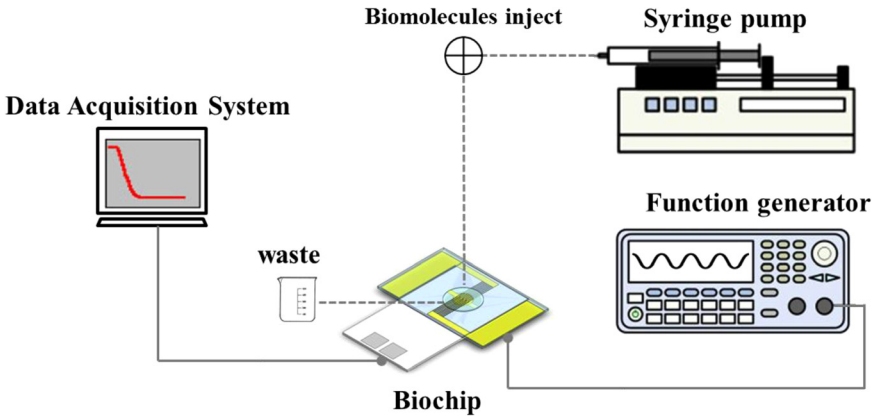

FIG. 2. Schematic diagram of the experimental setup.

bead (20 nm and 1 μm) is 1.05 g/cm^3.The water used to prepare all solutions was obtained from a Milli-Q water purification system (USA).

C. Functionalization of QCM and experimental procedure

The AT-cut QCM chips (ANT Technologies Corp., Taiwan) were used in the experiment. The quartz crystal and Au electrode had diameters of 7.2 mm and 3.6 mm, respectively, and the resonance frequency was 9 MHz. The QCM chips were processed using UV-Ozone cleaners to eliminate organic contaminants. The chips were then separately immersed in 1.2 M NaOH and 1.2 M HCl solution for 30 min, washed with deionized (DI) water, and stored in pure ethanol (>99.8 %) for later use. In this study, the well bonded cysteamine self-assembled monolayers (SAMs) with glutaraldehyde cross-linking layer was proposed for the immobilization of the amine latex bead. Figure 1(f) illustrates the binding process. The Au electrode of QCM chips were modified by 3 h of soaking in a 20 mM SAM of cysteamine (as linker) in ethanol followed by rinsing with ethanol and DI water. Finally, the chips were dried with N_2 gas. The reaction of cysteamine with the sensor surface in this step yielded free-amine-functional groups for further reaction.

The cysteamine-modified QCM chip and microelectrodes fabricated were assembled as the reaction sensing chamber. The phosphate-buffered saline used as the running buffer had a conductivity of 1.45 S/m as measured with a portable conductivity meter (SC-120; Suntex, Taiwan). Next, 500 μl of an activator 2.5 % glutaraldehyde (as ligand) in DI water were injected into the ETE-QCM chamber through inlet port at a flow rate of 20 μl/min. Glutaraldehyde was used as a homo-bifunctional crosslinker between the cysteamine-modified surface and the amine latex bead. In the following step, amine latex beads suspended in PBS were injected into the ETE-QCM chamber at a flow rate of 20 μl/min. The amine latex beads used were 20-nm (at concentrations of 10^{13} and 10^{14} spheres/ml) and 1-μm (at concentrations of 10^8 and 10^9 spheres/ml), respectively. Before injection, amine latex beads were separately agitated in a vortex stirrer and ultrasonicated for 5 min to prevent particle aggregation and to ensure concentration uniformity. After injecting the beads, the reaction chamber was completely filled with the bead solution after 30 s. The flow rate was then reduced to zero within 2 min by turning off the syringe pump; overall, 30 μl of beads were injected (internal volume of the reaction chamber was 6 μl). The fluid in the reaction chamber was kept in static state. Then two sets of experiments were performed. First, as a control set, the resonance frequencies of QCM chip were recorded for 20 min without activating ETE. The resonance frequency shifts due to the increased immobilized sensor surface density were totally relied on the pure diffusion of the suspended beads. In the second set of experiments, the first 10 min proceeded the same as the control set. Then, the function generator was turned on to activate ETE for 5 min. In the meantime, to mitigate interference caused by the AC voltage during signal recording, the QCM resonance frequency was not measured until when the generator was switched off. Signals were started to measure again (within 5 s when the generator was switched off) for 5 min. Each set of experiments was repeated at least six times to verify the reproducibility of the experiments. All experiments were performed at room temperature $(25 \pm 1.5)^{\circ}$C.

In the detection process, the frequency change was observed in a real-time continuous reading. When detecting analytes in liquid environments, both mass and liquid contribute to the total frequency change. Martin[44] derived the equation for the total frequency change and specified the simultaneous contribution of mass and liquid loading to the sensor signal:

$$\Delta F = -\frac{2f_0^2}{\sqrt{\mu_q \rho_q}} \frac{\Delta m}{A} - f_0{}^{3/2} \left(\frac{\Delta \rho_l \Delta \eta_l}{\mu_q \eta_q} \right)^{1/2}, \tag{2}$$

where f_0 is the resonance frequency, A is the area of the active crystal on the electrodes, ρ_q is the quartz crystal density (2.648 g/cm^3), μ_q is the shear modulus of the quartz crystals (2.947×10^{11} dyn/cm^2), ρ_l is the density of the liquid, η_l is the viscosity of the liquid, and Δm

is the adding mass on the crystal surface due to specific binding, respectively. The mass loading of immobilization of the amine latex bead contributes to frequency changes; however, the liquid loading does not. A 1 Hz change in resonance frequency corresponds to a 0.55 ng change in mass.

D. Electrothermal flow measurement

Electrothermally generated flow fields were observed using 4.5 μm latex beads (Thermo Scientific, USA) in PBS. Top views of the beads in the reaction chamber were observed and imaged with an upright fluorescence microscope (model BX 51, Olympus, Tokyo) and a computer with Olympus DP controller image software. After adding 1 μm fluorescent tracers (Invitrogen Molecular Probes, USA), their trajectories in the vortex were recorded. A particle tracking velocimetry (PTV) program was incorporated in MATLAB (Mathworks, Natick, MA, USA) for image processing. Finally, the time interval ($\Delta t = 1/30$ s) at which images were captured and the pixel of the moving tracers were used to calculate the vortex velocity.

E. SEM

A field emission SEM (S-4800, FE-SEM; Hitachi High-Technologies, Tokyo, Japan) was used for structural observation of the QCM sensor surfaces modified by 20-nm and 1-μm amine latex particles at varying magnifications. The SEM images were acquired at an acceleration voltage of 15 kV and a current of 10 μA.

III. NUMERICAL SIMULATIONS

Simulation of ETE was performed using the commercial software package COMSOL Multiphysics (COMSOL, Inc., Stockholm, Sweden) to yield the temperature and flow fields. The simulation results were helpful to confirm the correctness of the experimental data in the works. The finite element method and three-dimensional grid were employed to solve the governing equation. The procedure of numerical simulation for the electrothermal force was shown in many literatures[5,33] and our previous works.[45,46] Since our purpose in numerical simulation

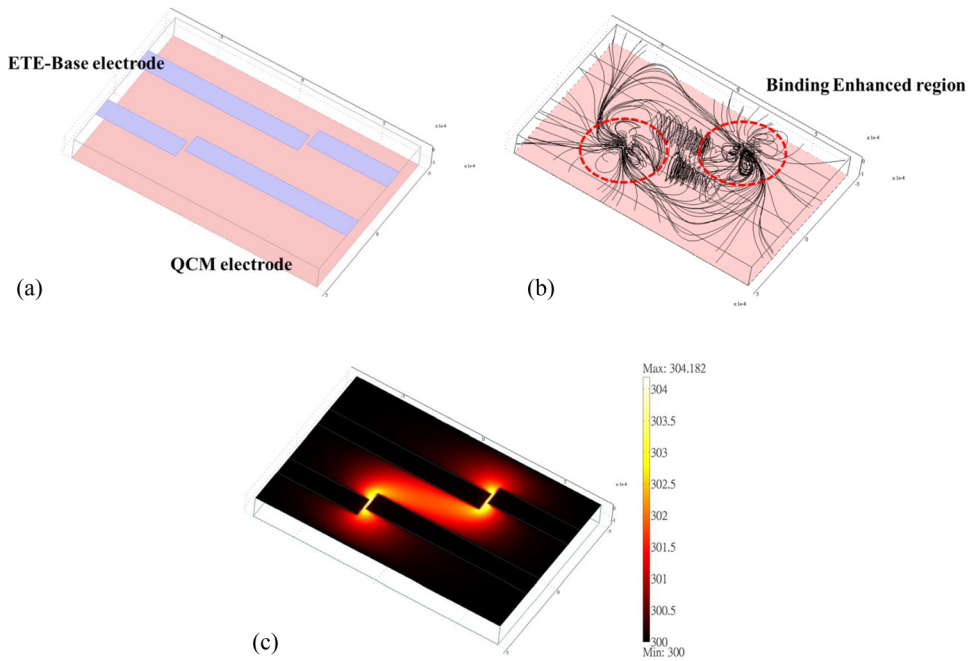

FIG. 3. (a) A simplified 3-D model block in the ETE-QCM chip. (b) Electrothermal vortices are produced below the top microelectrodes. (c) A maximum temperature increase of 4.18 K is achieved by applying 10 V_{pp} on the top electrodes.

was to view the local vortex flow field and temperature field near the electrodes created by ETE, a simplified 3-D block including only two pair of microelectrodes in the ETE-QCM chip was adopted, as shown in Figure 3(a). The dimensions of the block are 1500 μm $\times$ 500 μm $\times$ 150 μm. The two neighboring microelectrode pairs and the QCM electrode were placed on the top and bottom walls of the chamber, respectively. Figure 1(b) shows the geometry of the two neighboring microelectrode pairs. For the physical properties related to the electric field, flow field, and temperature field, the relative permittivity, the electrical conductivity, the density, the dynamic viscosity, the specific heat, and the thermal conductivity are 80.2, 1.45 S/m, 1×10^3 kg/m^3, 1×10^{-3} Pa $\cdot$ s, 4184 J/(kg $\cdot$ K), and 0.6 W/m $\cdot$ K, respectively. The boundary conditions for the electric field were applied voltage at the microelectrodes and electrically insulated elsewhere. The boundary conditions for the temperature field were temperature $T = 300$ K, at the top of the microelectrodes and at the bottom of QCM electrode. The remaining top was kept thermally insulated, and the four side boundaries were set as convective heat flux. The boundary conditions for the flow field were pressure $p = 0$ at the four side boundaries and non-slip elsewhere.

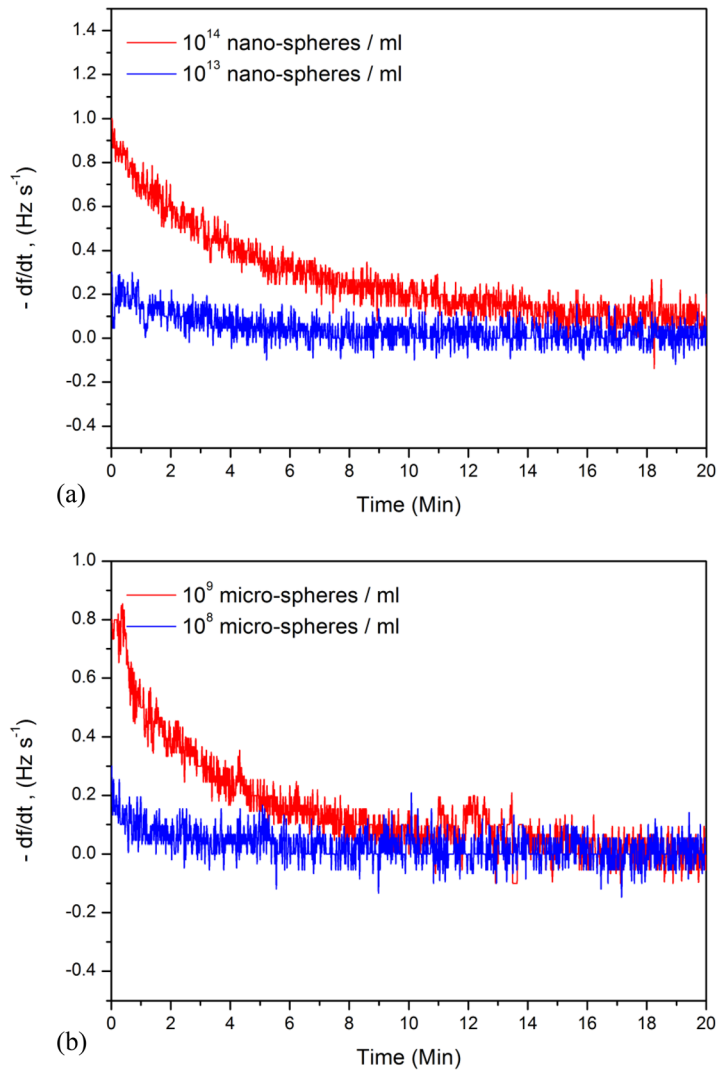

FIG. 4. (a) and (b) The injection of 20 nm and 1 μm amine latex beads into the reaction chamber. In the absence of electrothermal force, the binding rate decelerated with time. Thus, electrothermal flow was initiated after 10 min to measure the increased binding capacity resulting from the electrothermal vortex.

IV. RESULTS AND DISCUSSION

A. Electrothermally induced flow

Electrolysis of the electrode or bubbles can distort the QCM signal. Thus, the AC voltage was set to 10 V_{pp} and 10 MHz to assure that the microelectrodes developed in this study could generate a vortex without inducing electrolysis or bubbles (see the supplementary material).[47] Maximum velocity of the vortex was 383 μm/s by the PTV measurements. Figure 3(b) shows the simulation results for fluid motion with streamlines. The maximum velocity in simulation is about 260 μm/s. The simulated velocity data were at the order of hundreds of μm/s, which were directly comparable to the experiment data. Obviously, the electrothermal vortex flow will drive the flow toward the sensor surface, tear the diffusion boundary layer, and accelerate the specific binding of analytes and ligands on the sensing area.

B. The effect of diffusion on binding rate

The experiment was performed using amine latex beads with two diameters of 20 nm and 1 μm, respectively. Figures 4(a) and 4(b) show the binding rates for the 20 nm amine latex beads (10^{13}–10^{14} spheres/ml) and 1 μm amine latex beads (10^{8}–10^{9} spheres/ml), respectively. Since in this stage the fluid in the chamber was kept in static state, the specific binding rate depended fully on the diffusion of the suspended analytes. It was seen that the binding rate decreased as time increased. Around 5 min later, the binding rate of 10^{13}-spheres/ml beads was rather slow; in contrast, the 10^{14}-spheres/ml beads required about 10 min to reach a low binding rate because of the higher concentration. The low binding rate resulted from slow diffusion rather than from saturation of the binding reaction between analytes and ligands. Next, in both cases, ETE was applied from 10th to 15th min to generate electrothermal flow, and so the major contribution of the binding rate was assured to come from ETE. In Sec. IV C, changes in the resonance frequency of QCMs were compared in the presence and absence of ETE.

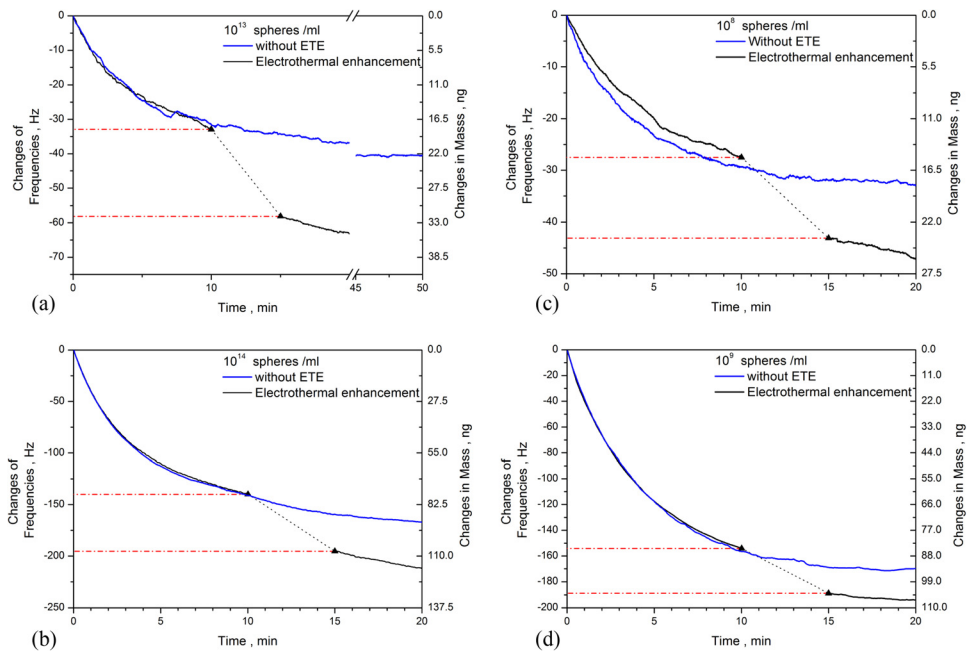

FIG. 5. (a) and (b) Signals for 20 nm beads at concentrations of 10^{13} and 10^{14} spheres/ml. When the binding rate decelerated, a 5 min application of AC voltage yielded resonance frequency variations of 25.2 and 55.4 Hz, respectively, while those in the control group without electrothermal effects were 2.6 and 18.3 Hz, respectively. (c) and (d) Signals for 1 μm beads at concentrations of 10^{8} and 10^{9} spheres/ml. When the binding rate decelerated, a 5 min application of AC voltage yielded resonance frequency variations of 15.6 and 34.6 Hz, respectively, while those in the control group without ETE were 2.6 and 12.4 Hz, respectively.

C. Quantitative analysis of ETEs of QCM signals

The QCM resonance frequency measurement was experimentally applied to determine the effects of electrothermal stirring on analyte binding capacity. The AC voltage caused interference to the QCM oscillator circuit and further affected the measurement stability. Hence, the measurement was stopped when the electrothermal effect was activated, and the resonance frequency reading was resumed immediately after the electrothermal effect was turned off. In Figure 5(a), when the binding rate of 10^{13}-spheres/ml beads decreased to a relatively low binding rate (at 10th minutes after the syringe pump was switched off). After applying 5 min (from 10th to 15th min) ETE, the beads yielded a QCM frequency variation of 24.6 ± 4.9 Hz. In contrast, the diffusion effects (for the same amount of time) generated a frequency variation of 2.7 ± 0.5 Hz (Figure 6(a)). These experimental results indicated that ETE drived particles to bind to the sensor surface. Additionally, calculations revealed that the electrothermal force obtained a mass change of 13.5 ng, which was superior to the mass change of 1.5 ng obtained by pure diffusion. Figure 5(b) presents the QCM signals of 10^{14}-spheres/ml beads. In the absence of ETE (the period between 10th and 15th min), the frequency variation was 18.1 ± 3.6 Hz, which corresponded to a mass change of 10.0 ng

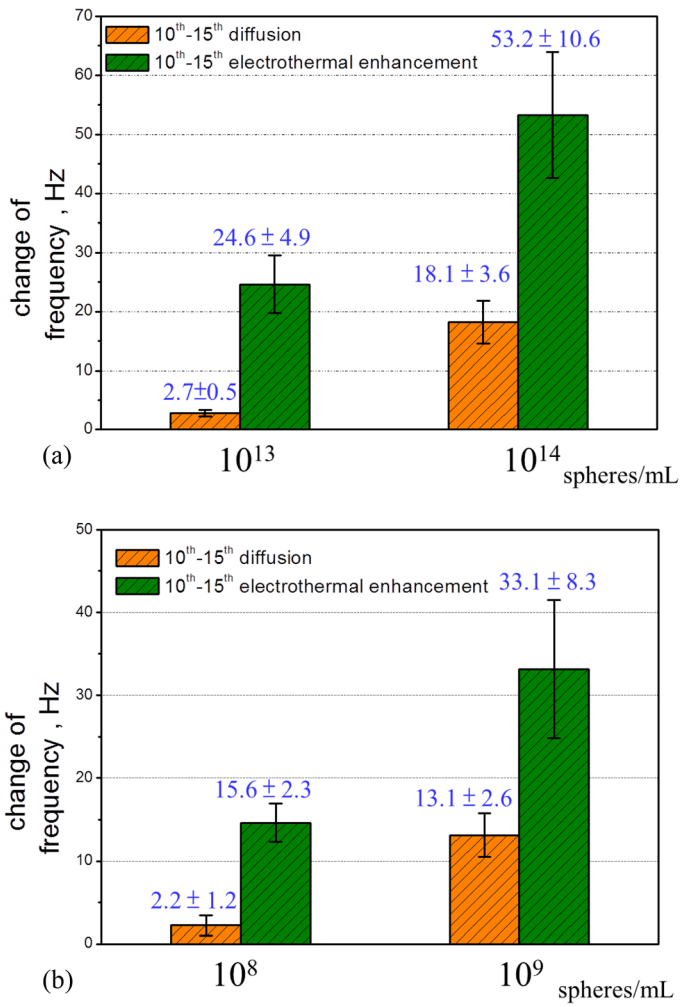

FIG. 6. Comparison of frequency variations in (a) 20 nm beads and (b) 1 μm beads after 10th–15th min exposure to electrothermal and diffusion effects (frequency variation is expressed in terms of mean ± standard deviation, n = 6). A two-tailed Student's t test was used to compare the experimental and control groups. The statistical results were determined as significantly different with a p-value <0.01 for all our four sets of experimental data.

whereas electrothermal mixing yielded a variation of 53.2 ± 10.6 Hz which corresponded to a mass change of 29.3 ng (Figure 6(a)). Compared with the control group, the net contribution of electrothermal mixing yielded an additional frequency variation of approximately 35 Hz equivalent to a mass change of 19.3 ng. Thus, electrothermal stirring immediately enhanced analyte binding whereas diffusion alone required a prolonged period ($\gg$30 min, Figure 5(a)).

Figures 5(c) and 5(d) display the experimental results for 1-μm beads in concentrations of 10^8 and 10^9 spheres/ml. Because 1 μm particle was heavier than a 20-nm particle, a lower concentration range was examined. In the absence of electrothermal force in the period between 10th and 15th min, diffusion effects caused frequency variations of 2.2 ± 1.2 and 13.1 ± 2.6 Hz

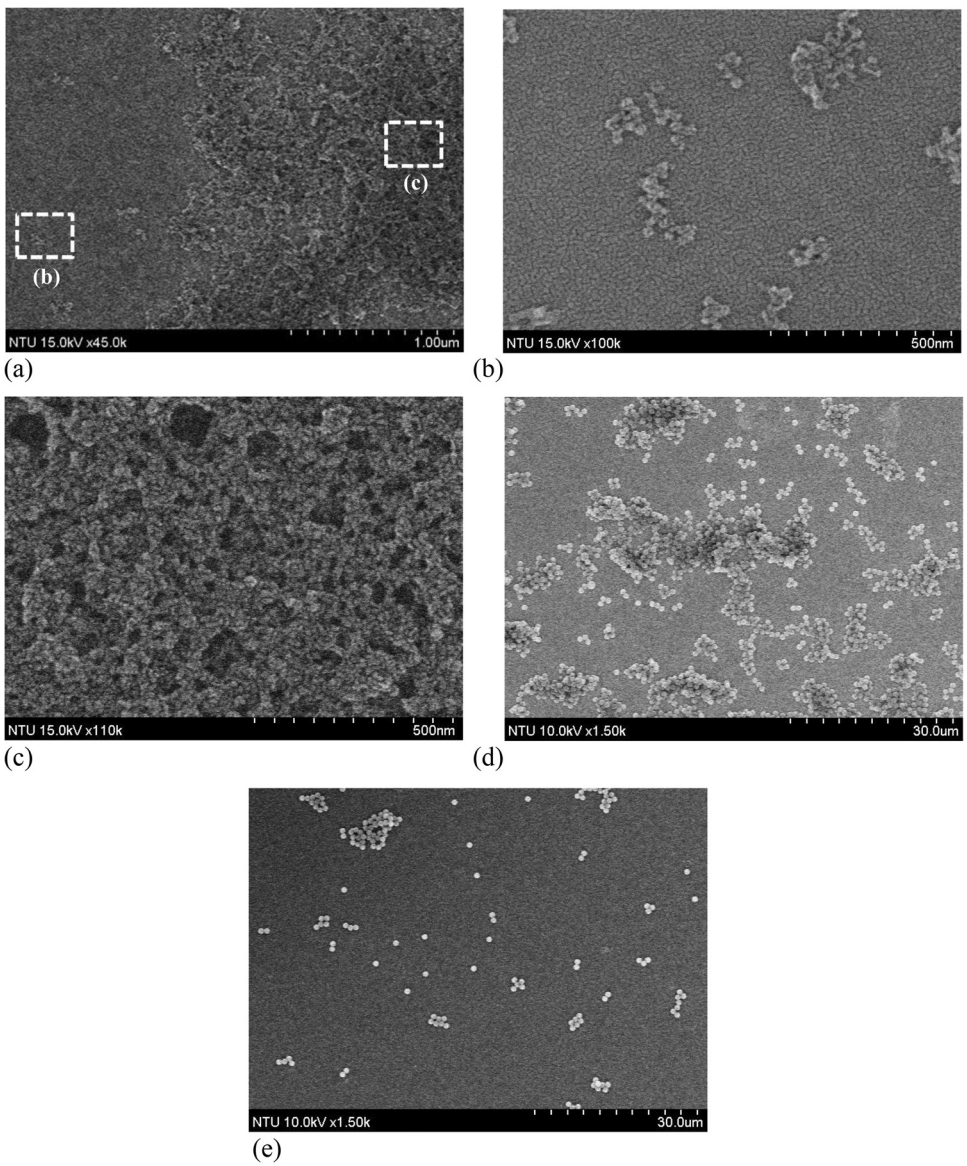

FIG. 7. (a) The 20 nm beads were concentrated on the sensor surface (right hand side of the diagram) near the electrothermal vortex because electrothermal mixing increased contact between the analytes and ligands. The left side of the diagram shows that few beads bound to the surface without electrothermal vortex because diffusion was dominant in this region. (b) and (c) Magnification of images on the left and right side of (a). The 1-μm latex beads at a concentration of 10^9 spheres/ml were bound to the sensor surface in regions (d) under and near the electrothermal vortex and (e) in regions unaffected by the electrothermal vortex.

for the 10^8- and 10^9-spheres/ml beads (Figure 6(b)), which were equivalent to mass increases of 1.2 ng and 7.2 ng, respectively. For the same durations, ETE generated variations of 15.6 ± 2.3 and 33.1 ± 8.3 Hz, which were equivalent to mass increases of 8.4 ng and 18.2 ng, respectively (Figure 4(b)). The experimental results indicated that the electrothermally induced flow effectively convected the suspended analytes to the sensor surface.

The average of temperature rise of 3.5 K within fluid around the gap of the electrodes was recorded using a thermometer (822; YOTEC, Taiwan) when electrothermal effect was activated for 5 min. When the generator was switched off, the temperature decreased immediately and returned to room temperature within 90 s. The QCM sensing electrodes acted as a heat sink by transmitting Joule heat generated in the reaction chamber to the external environment through a conducting wire.[48] Simulation results indicated that the maximum steady state temperature rise was approximately 4.18 K at the microelectrode gap, where electric fields were concentrated (Fig. 3(c)).

D. Scanning electron microscopy

Figures 7(a)–7(e) show SEM images of binding in the 10^{13}-spheres/ml (diameter 20-nm) and 10^9-spheres/ml (diameter 1-μm) beads after 5 min of electrothermal stirring. Vortexing concentrated particles in the lower section of the sensing electrodes (under the vortex indicated by dashed lines in Fig. 1(a)), which demonstrated that electrothermal mixing enhanced the binding capacity of the particles. Away from the vortex, particles movement was caused only by diffusion; therefore, particle binding in this region was limited. The SEM images indicated that ETE did improve the performance of the QCM sensor.

V. CONCLUSION

In this work, a new integrated biosensor system composed of QCM and ETE devices was performed experimentally to investigate the performance enhancement of QCM by ETE. The electrothemal vortex flow generated by ETE electrodes provided additional power to drive the suspended analytes in the fluid moving toward the sensor surface. In contrast to the static fluid in the reaction chamber, the ETE in the setup of this work was measured to yield a maximum flow velocity of 383 μm/s after applying an AC voltage of 10 V_{pp} and 10 MHz. By using a microchannel to analyze the biosensor performance in a closed system, sensing signals were directly measured in the liquid phase. As control groups, blank experiments without applying ETE were also done for the purpose of comparisons. Amine latex beads as analytes (diameter, 20 nm and 1 μm) were used in the experiments. In the case of 20-nm amine latex beads in ETE phase, the resonant frequency variations at concentrations of 10^{13} and 10^{14} spheres/ml were 24.6 ± 4.9 and 53.2 ± 10.6 Hz, respectively. In the control group without ETE, the respective variations were 2.7 ± 0.5 Hz and 18.1 ± 3.6 Hz, respectively. In the case of 1-μm amine latex beads with ETE, the resonant frequency variations at concentrations of 10^8 and 10^9 spheres/ml were 15.6 ± 2.3 and 33.1 ± 8.3 Hz, respectively, while those in the control group without ETE were 2.2 ± 1.2 Hz and 13.1 ± 2.6 Hz, respectively. In addition, a 3.5 K temperature rise in the fluid near the electrode gap was measured after ETE had been applied. The experimental work in this study revealed that ETE significantly enhanced the amine latex bead specific binding on the QCM biosensor resulting in much larger resonance frequency variations, which were also verified by the observation of the increased binding density on the sensor surface of the QCM through SEM images. A numerical simulation was also done to obtain the temperature and vortex flow fields due to ETE. The maximum temperature rise by simulation was 4.18 K and the elctrothermal vortices were confined to the region near electrode gaps, which was consistent with the distribution of the immobilized sensor surface density observed on the SEM images. The experimental results indicated that the electrothermally induced flow can effectively mix the nanoscale and microscale particles. Thus, in both antibody immunoassays and cell interaction analysis, ETE is applicable for analyzing the binding and killing activities of immune and cancer cells.[49]

ACKNOWLEDGMENTS

The authors would like to thank the Ministry of Science and Technology of Taiwan for financially supporting this research under Contract No. MOST 103-2221-E-002-035 and the Nano-Electro-Mechanical-System (NEMS) Research Center at National Taiwan University for the use of the MEMS facilities.

[1]S. Kuan, S.-C. Chi, Y.-J. Cheng, T.-J. Chia, and L.-S. Huang, "Binding kinetics of grouper nervous necrosis viruses with functionalized antimicrobial peptides by nanomechanical detection," Biosens. Bioelectron. **31**, 116–123 (2012).
[2]L. A. Su, W. Z. Jia, C. J. Hou, and Y. Lei, "Microbial biosensors: A review," Biosens. Bioelectron. **26**, 1788–1799 (2011).
[3]J. R. Chen, Y. Q. Miao, N. Y. He, X. H. Wu, and S. J. Li, "Nanotechnology and biosensors," Biotechnol. Adv. **22**, 505–518 (2004).
[4]W. M. Deen, *Analysis of Transport Phenomena* (Oxford University Press, New York, 1998).
[5]M. Sigurdson, D. Z. Wang, and C. D. Meinhart, "Electrothermal stirring for heterogeneous immunoassays," Lab Chip **5**, 1366–1373 (2005).
[6]G. Q. Hu, Y. L. Gao, and D. Q. Li, "Modeling micropatterned antigen-antibody binding kinetics in a microfluidic chip," Biosens. Bioelectron. **22**, 1403–1409 (2007).
[7]D. B. Hibbert, J. J. Gooding, and P. Erokhin, "Kinetics of irreversible adsorption with diffusion: Application to biomolecule immobilization," Langmuir **18**, 1770–1776 (2002).
[8]C.-K. Yang, J.-S. Chang, S. D. Chao, and K.-C. Wu, "Two dimensional simulation on immunoassay for a biosensor with applying electrothermal effect," Appl. Phys. Lett. **91**, 113904 (2007).
[9]P. K. Wong, T. H. Wang, J. H. Deval, and C. M. Ho, "Electrokinetics in micro devices for biotechnology applications," IEEE/Asme Trans. Mechatron. **9**, 366–376 (2004).
[10]M. P. Hughes, "AC electrokinetics: applications for nanotechnology," Nanotechnology **11**, 124–132 (2000).
[11]C.-P. Jen and H.-H. Chang, "A handheld preconcentrator for the rapid collection of cancerous cells using dielectrophoresis generated by circular microelectrodes in stepping electric fields," Biomicrofluidics **5**, 034101 (2011).
[12]C.-P. Jen and T.-W. Chen, "Selective trapping of live and dead mammalian cells using insulator-based dielectrophoresis within open-top microstructures," Biomed. Microdevices **11**, 597–607 (2009).
[13]C.-P. Jen and W.-F. Chen, "An insulator-based dielectrophoretic microdevice for the simultaneous filtration and focusing of biological cells," Biomicrofluidics **5**, 044105 (2011).
[14]W. Y. Ng, S. Goh, Y. C. Lam, C. Yang, and I. Rodriguez, "DC-biased AC-electroosmotic and AC-electrothermal flow mixing in microchannels," Lab Chip **9**, 802–809 (2009).
[15]Q. Yuan and J. Wu, "Thermally biased AC electrokinetic pumping effect for Lab-on-a-chip based delivery of biofluids," Biomed. Microdevices **15**, 125–133 (2013).
[16]P. Yager, T. Edwards, E. Fu, K. Helton, K. Nelson, M. R. Tam *et al.*, "Microfluidic diagnostic technologies for global public health," Nature **442**, 412–418 (2006).
[17]J. Oh, R. Hart, J. Capurro, and H. Noh, "Comprehensive analysis of particle motion under non-uniform AC electric fields in a microchannel," Lab Chip **9**, 62–78 (2009).
[18]C.-T. Huang, C.-H. Weng, and C.-P. Jen, "Three-dimensional cellular focusing utilizing a combination of insulator-based and metallic dielectrophoresis," Biomicrofluidics **5**, 044101 (2011).
[19]M. Koklu, S. Park, S. D. Pillai, and A. Beskok, "Negative dielectrophoretic capture of bacterial spores in food matrices," Biomicrofluidics **4**, 034107 (2010).
[20]E. M. Melvin, B. R. Moore, K. H. Gilchrist, S. Grego, and O. D. Velev, "On-chip collection of particles and cells by AC electroosmotic pumping and dielectrophoresis using asymmetric microelectrodes," Biomicrofluidics **5**, 034113 (2011).
[21]M. L. Y. Sin, V. Gau, J. C. Liao, and P. K. Wong, "Electrothermal fluid manipulation of high-conductivity samples for laboratory automation applications," JALA **15**, 426–432 (2010).
[22]A. Castellanos, A. Ramos, A. Gonzalez, N. G. Green, and H. Morgan, "Electrohydrodynamics and dielectrophoresis in microsystems: Scaling laws," J. Phys. D: Appl. Phys. **36**, 2584–2597 (2003).
[23]A. Ramos, H. Morgan, N. G. Green, and A. Castellanos, "Ac electrokinetics: A review of forces in microelectrode structures," J. Phys. D: Appl. Phys. **31**, 2338–2353 (1998).
[24]R. An, D. O. Wipf, and A. R. Minerick, "Spatially variant red blood cell crenation in alternating current non-uniform fields," Biomicrofluidics **8**, 021803 (2014).
[25]N. S. K. Gunda, S. Bhattacharjee, and S. K. Mitra, "Study on the use of dielectrophoresis and electrothermal forces to produce on-chip micromixers and microconcentrators," Biomicrofluidics **6**, 034118 (2012).
[26]C. Meinhart, D. Z. Wang, and K. Turner, "Measurement of AC electrokinetic flows," Biomed. Microdevices **5**, 139–145 (2003).
[27]J. Cao, P. Cheng, and F. J. Hong, "A numerical study of an electrothermal vortex enhanced micromixer," Microfluid. Nanofluid. **5**, 13–21 (2008).
[28]C. K. Yang, J. S. Chang, S. D. Chao, and K. C. Wu, "Effects of diffusion boundary layer on reaction kinetics of immunoassay in a biosensor," J. Appl. Phys. **103**, 084702 (2008).
[29]K. R. Huang, J. S. Chang, S. D. Chao, T. S. Wung, and K. C. Wu, "Study of active micromixer driven by electrothermal force," Jpn. J. Appl. Phys. **51**, 047002 (2012).
[30]J. J. Feng, S. Krishnamoorthy, and S. Sundaram, "Numerical analysis of mixing by electrothermal induced flow in microfluidic systems," Biomicrofluidics **1**, 024102 (2007).
[31]J. A. Wood, B. Zhang, M. R. Tomkins, and A. Docoslis, "Numerical investigation of AC electrokinetic virus trapping inside high ionic strength media," Microfluid. Nanofluid. **3**, 547–560 (2007).
[32]K. R. Huang, Z. H. Hong, and J. S. Chang, "Microfluidic mixing on application of traveling wave electroosmosis," Eur. J. Mech. B. Fluids **48**, 153–164 (2014).

[33]H. C. Feldman, M. Sigurdson, and C. D. Meinhart, "AC electrothermal enhancement of heterogeneous assays in microfluidics," Lab Chip **7**, 1553–1559 (2007).
[34]R. Hart, E. Ergezen, R. Lec, and H. Noh, "Improved protein detection on an AC electrokinetic quartz crystal microbalance (EKQCM)," Biosens. Bioelectron. **26**, 3391–3397 (2011).
[35]M. X. Ouyang, R. Mohan, Y. Lu, T. T. Liu, K. E. Mach, M. L. Y. Sin *et al*., "An AC electrokinetics facilitated biosensor cassette for rapid pathogen identification," Analyst **138**, 3660–3666 (2013).
[36]N. Islam, M. Lian, and J. Wu, "Enhancing microcantilever capability with integrated AC electroosmotic trapping," Microfluid. Nanofluid. **3**, 369–375 (2007).
[37]M. Lazerges, H. Perrot, N. Zeghib, E. Antoine, and C. Compere, "*In situ* QCM DNA-biosensor probe modification," Sens. Actuators, B **120**, 329–337 (2006).
[38]R. E. Baltus, K. S. Carmon, and L. A. Luck, "Quartz crystal microbalance (QCM) with immobilized protein receptors: Comparison of response to ligand binding for direct protein immobilization and protein attachment via disulfide linker," Langmuir **23**, 3880–3885 (2007).
[39]P. J. Liao, J. S. Chang, S. D. Chao, H. C. Chang, K. R. Huang, K. C. Wu *et al*., "A combined experimental and theoretical study on the immunoassay of human immunoglobulin using a quartz crystal microbalance," Sensors **10**, 11498–11511 (2010).
[40]A. J. C. Eun, L. Q. Huang, F. T. Chew, S. F. Y. Li, and S. M. Wong, "Detection of two orchid viruses using quartz crystal microbalance (QCM) immunosensors," J. Virol. Methods **99**, 71–79 (2002).
[41]C. F. Lee, T. R. Yan, and T. H. Wang, "Long-term monitoring of Caco-2 cell growth process using a QCM-cell system," Sens. Actuators, B **166**, 165–171 (2012).
[42]Q. D. Zhang, Y. Y. Huang, R. Zhao, G. Q. Liu, and Y. Chen, "Determining binding sites of drugs on human serum albumin using FIA-QCM," Biosens. Bioelectron. **24**, 48–54 (2008).
[43]L. Sartore, M. Barbaglio, L. Borgese, and E. Bontempi, "Polymer-grafted QCM chemical sensor and application to heavy metal ions real time detection," Sens. Actuators, B **155**, 538–544 (2011).
[44]S. J. Martin, V. E. Granstaff, and G. C. Frye, "Characterization of a quartz crystal microbalance with simultaneous mass and liquid loading," Anal. Chem. **63**, 2272–2281 (1991).
[45]K. R. Huang, J. S. Chang, S. D. Chao, K. C. Wu, C. K. Yang, C. Y. Lai *et al*., "Simulation on binding efficiency of immunoassay for a biosensor with applying electrothermal effect," J. Appl. Phys. **104**, 064702 (2008).
[46]K. R. Huang and J. S. Chang, "Three dimensional simulation on binding efficiency of immunoassay for a biosensor with applying electrothermal effect," Heat Mass Transfer **49**, 1647–1658 (2013).
[47]See supplementary material at http://dx.doi.org/10.1063/1.4898633 for experimental observation of electrothermal flow.
[48]V. Chaurey, C. Polanco, C.-F. Chou, and N. S. Swami, "Floating-electrode enhanced constriction dielectrophoresis for biomolecular trapping in physiological media of high conductivity," Biomicrofluidics **6**, 012806 (2012).
[49]L. Zamai, A. R. Mariani, G. Zauli, L. Rodella, R. Rezzani, F. A. Manzoli *et al*., "Kinetics of in vitro natural killer activity against K562 cells as detected by flow cytometry," Cytometry **32**, 280–285 (1998).